Accepted Manuscript

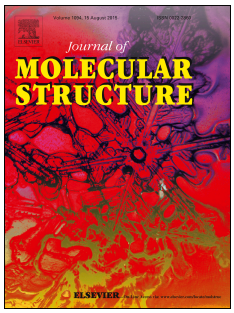

Structural, spectroscopic and microbiological characterization of the chalcone 2E-1-(2′-hydroxy-3′,4′,6′-trimethoxyphenyl)-3-(phenyl)-prop-2-en-1-one derived from the natural product 2-hydroxy-3,4,6-trimethoxyacetophenone

A.M.R. Teixeira, H.S. Santos, P.N. Bandeira, M.S.S. Julião, P.T.C. Freire, V.N. Lima, B.G. Cruz, P.T. da Silva, H.D.M. Coutinho, D.M. Sena, Jr.

PII: S0022-2860(18)31387-5

DOI: https://doi.org/10.1016/j.molstruc.2018.11.075

Reference: MOLSTR 25904

To appear in: *Journal of Molecular Structure*

Received Date: 17 August 2018

Revised Date: 15 November 2018

Accepted Date: 22 November 2018

Please cite this article as: A.M.R. Teixeira, H.S. Santos, P.N. Bandeira, M.S.S. Julião, P.T.C. Freire, V.N. Lima, B.G. Cruz, P.T. da Silva, H.D.M. Coutinho, D.M. Sena Jr., Structural, spectroscopic and microbiological characterization of the chalcone 2E-1-(2′-hydroxy-3′,4′,6′-trimethoxyphenyl)-3-(phenyl)-prop-2-en-1-one derived from the natural product 2-hydroxy-3,4,6-trimethoxyacetophenone, *Journal of Molecular Structure* (2018), doi: https://doi.org/10.1016/j.molstruc.2018.11.075.

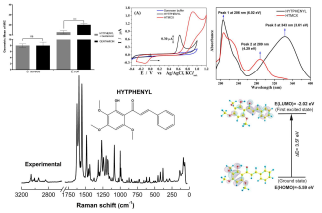

Structural, spectroscopic and microbiological characterization of the chalcone 2E-1-(2′-Hydroxy-3′,4′,6′-trimethoxyphenyl)-3-(phenyl)-prop-2-en-1-one derived from the natural product 2-hydroxy-3,4,6-trimethoxyacetophenone

A.M.R. Teixeira[a,b*], H.S. Santos[c], P.N. Bandeira[c], M.S.S. Julião[c], P.T.C. Freire[d], V.N. Lima[a], B.G. Cruz[a], P.T da Silva[a,c], H.D.M. Coutinho[a], D.M. Sena Jr.[a]

[a] Department of Biological Chemistry, Regional University of Cariri, Crato, CE, 63105-000, Brazil

[b] Department of Physics, Regional University of Cariri, Juazeiro do Norte, CE, 63041-145, Brazil

[c] Science and Technology Centre - Course of Chemistry, State University Vale do Acaraú, Sobral, CE, 62040-370, Brazil

[d] Department of Physics, Federal University of Ceará, Fortaleza, CE, 60455-760, Brazil

ABSTRACT

Chalcones are important intermediates in the biosynthesis of biologically active compounds such as flavonoids and their derivatives. In this paper, a new chalcone 2*E*-1-(2′-Hydroxy-3′,4′,6′-trimethoxyphenyl)-3-(phenyl)-prop-2-en-1-one (HYTPHENYL) was synthesized by the condensation reaction of Claisen-Schmidt in basic medium between the 2-hydroxy-3,4,6-trimethoxyacetophenone (HTMCX) and benzaldehyde. The molecular structure of this chalcone was determined by Nuclear Magnetic Resonance, and characterized by infrared and Raman spectroscopy, at room temperature. Its electrochemical behavior was also evaluated. Vibrational wavenumber and wavevector have been predicted using the Density Functional Theory (DFT) calculations and their normal modes were analyzed in terms of the potential energy distribution (PED). Furthermore, DFT calculations were carried out to obtain the molecular orbitals and the electrostatic surface map. Electronic absorption spectrum of HYTPHENYL was measured and compared with that obtained for the HTMCX compound. Additionally, analysis of the antimicrobial activity and antibiotic resistance

[*]Corresponding author. FAX: 55-88-3102 1294, Phone: 55-85-999 224809.

E-mail address: alexandre.teixeira@urca.br

modulation was carried out to evaluate the antibacterial potential of the HYTPHENYL chalcone.

Keywords: NMR; Vibrational spectroscopy; UV-VIS; DFT; Voltammetric study, Antimicrobial activity; Chalcone.

1. Introduction

The chalcones and their derivatives have received great attention because of their simple structure and the diversity of pharmacological activities that they present [1-10]. Among them, we can mention anti-cancer [4, 11-13], antioxidant [12], anti-HIV [14], antibacterial [15, 16], antimalarial [17], anti-infective [18], anti-inflammatory [18] activities, inhibitors of tyrosine phosphatase A of *Mycobacterium tuberculosis* [19], and antifungal [20].

Recently, we have published a paper on antimicrobial and modulatory activities of the compound 2-hydroxy-3,4,6-trimethoxyacetophenone ($C_{11}O_5H_{14}$, hereafter named HTMCX) isolated of the stem bark of *Croton anisodontus* [21]. The results from the work of Ref. [21] indicated that this natural compound, when associated with amikacin antibiotic, presents synergism against *Pseudomonas aeruginosa* 03 and *Staphylococcus aureus* 358. These results corroborate with other reports in the literature that combine natural products with antibiotics against bacteria to decrease microbial resistance [22]. Furthermore, the synthesis of analogues [23, 24] and derived from the natural products [24] may enable the discovery of new active substances. In this context, we have synthesized a new chalcone from natural product HTMCX. Also, very recently, we have reported a complete study of the structural and vibrational properties of this natural product [25].

In this paper, a new chalcone 2*E*-1-(2′-Hydroxy-3′,4′,6′-trimethoxyphenyl)-3-(phenyl)-prop-2-en-1-one ($C_{18}O_5H_{18}$, hereafter named HYTPHENYL) was synthesized by the condensation reaction of Claisen-Schmidt [26] in basic medium between the natural compound HTMCX and benzaldehyde. The molecular structure of this chalcone was determined by Nuclear Magnetic Resonance, and characterized by infrared and Raman spectroscopy, at room temperature. Its electrochemical behavior was also evaluated. Vibrational wavenumber and wavevector were predicted using the Density Functional Theory (DFT) calculations and their normal modes were analyzed in terms

of the potential energy distribution (PED). Furthermore, DFT calculations were carried out to obtain the molecular orbitals and the electrostatic surface map. Electronic absorption spectrum of HYTPHENYL was measured and compared with that obtained for the HTMCX. Additionally, analysis of the antimicrobial activity and antibiotic resistance modulation was carried out to evaluate the antibacterial potential of the HYTPHENYL chalcone. Literature survey reveals that to the best of our knowledge neither the structural, electrochemical and vibrational properties of chalcone HYTPHENYL nor the study of antimicrobial activity and modulatory antimicrobial activity for the HYTPHENYL compound were reported yet. Beyond a complete characterization of the material, our study points to the potential use of this chalcone in synergy with antibiotics as antimicrobial agent.

2. Materials and methods

2.1 Synthesis of the chalcone HYTPHENYL

The chalcone synthesis is as shown in Figure 1. The starting materials were the natural product 2-Hydroxy-3,4,6-trimethoxyacetophenone (HTMCX) (**1**) and benzaldehyde (**2**) commercially obtained from Sigma-Aldrich. The chalcone derivative (**3**) was prepared by stirring a solution of HTMCX compound **(1)** (0.20g; 0.62 mmol), EtOH (10 mL), NaOH (0.25g; 6,5 mmol), and benzaldehyde (0.1093g; 1.03 mmol) **(2)** at room temperature for 2 h. The NMR data confirm that the product of this synthesis is the chalcone 2*E*-1-(2′-Hydroxy-3′,4′,6′-trimethoxyphenyl)-3-(phenyl)-prop-2-en-1-one (HYTPHENYL).

2.2 NMR data of the chalcone HYTPHENYL

^{1}H-NMR showed peaks at δ_H 3.96 ppm (s) and 3.85 ppm (s) corresponding to hydrogen atoms from three methoxy groups. The resonances at δ_H 6.01 (s) is due to the only hydrogen atom bound to the aromatic ring, and the one at δ_H 13.94 (1H, s) is due to a chelated phenol hydroxyl group. Additionally, the signals at δ_H 7.79 and 7.88 ppm are attributed to hydrogens α and β, respectively. ^{13}C-NMR and DEPT 135° allowed to recognize signals for three methoxy groups at δ_C 60.94, 56.26 and 56.22 ppm, six aromatic quaternary carbon atoms with peaks at δ_C 159.6 (C-4´), 158.8 (C-6´), 158.7 (C-2´), 131.2 (C-5´), 107.1 (C-1´) and 135.7 (C-1), six aromatic methines carbon at δ_C

130,3 (C-4), 129.1 (C-3/5), δ_C 128.6 (C-2/6) and 87.4 (C-3´). Additionally, the signal at δ_C 193.5 ppm suggests the presence of one conjugated carbonyl group and the signals at δ_C 127.7 and $_{\delta C}$ 142.8 ppm should be associated with C-sp^2. The NMR spectra of the ^{13}C (125 MHz) and ^{1}H (500 MHz) in ($CDCl_3$, δ, ppm, J/Hz) are presented in the Supplementary Material on Figure S1 and Figure S2, respectively.

2.3 Raman, IR, UV-VIS measurements

FT-Raman spectra were taken using a Bruker RFS100/S FTR system and a D418-T detector, with the sample excited by means of the 1064 nm line of a Nd:YAG laser. FT-Raman spectrum was collected from samples confined in screw cap standard chromatographic glass vials, at a nominal resolution of 4 cm^{-1} accumulating 60 scans per spectra and using a laser power of 150 mW.

The infrared spectra were obtained by using a Cary 660 FT-IR spectrometer. In order to record IR spectra we have grinded the sample in an agate mortar to minimize scattering on the particle surface and prepared a pellet with KBr by mixing it with the sample until a uniform mixture was obtained.

The UV absorption spectra of the HTMCX and HYTPHENYL compounds were recorded in ethanol on a GENESYS™ 10S UV-Vis spectrophotometer.

2.4 Computational method

Calculations using DFT were carried out with the Gaussian *09* programme package [27]. The B3LYP functional was used with the 6-31 G(d,p) basis set. The molecular structure of HYTPHENYL used as the input files for Gaussian was drawn in the ChemSketch program [28] by means of the data obtained from NMR data. The structure was optimized and the wavenumbers and the atomic displacements for each mode were then calculated. At the optimized structures of the molecules, the calculations do not furnish any imaginary frequency. The wavefunctions of electron densities were obtained for the optimized structure of HYTPHENYL compound. The wavefunctions generated were used for molecular electrostatic potential (MEP) calculations. Furthermore, DFT calculations were carried out to obtain the Kohn-Sham orbitals and the Highest Occupied Molecular Orbital (HOMO) and the Lowest Unoccupied Molecular Orbital (LUMO), as well as the following quantum chemical parameters: vertical ionization energy, vertical electron affinity, chemical potential, electronegativity, global hardness and electrophilicity index. To construct the MEP

surface and the shape of HOMO and LUMO orbitals, the Chemcraft program [29] was utilized. Theoretical Raman frequencies were scaled through least-square fits as suggested by Rauhut and Pulay [30]. For the HYTPHENYL compound we used the scaling factor of 0.9626 for frequencies below 2000 cm^{-1}, and for frequencies above 2000 cm^{-1}, the scaling factor was 0.9440. The description of the normal modes of vibration were made based on the potential energy distribution (PED) calculated using the program VEDA [31]. The calculated vibrational wavenumbers were adjusted to compare with experimental Raman and infrared frequencies.

2.5 Electrochemical measurements

The electrochemical investigation of chalcone HYTPHENYL was performed with a conventional three-electrode cell in an μAutolab III potentiostat (Metrohm Autolab BV, Utrecht, the Netherlands) coupled to a PC microcomputer, using NOVA 2.1.3. software. The working electrode was a glassy carbon electrode, GCE, (Metrohm Autolab BV) of 3 mm diameter, the counter electrode was platinum coil, and the reference electrode was Ag/AgCl, Cl^- (3.0 mol L^{-1}), all contained in one-compartment electrochemical cell with a volumetric capacity of 20.0 mL. It was used a volume of 10.0 mL. 0.25 mmol L^{-1} of HYTPHENYL and 3.0 mmol L^{-1} of acetophenone HTMCX stock solutions, prepared by dissolving 7.9 mg in 100 mL of ethanol and 33.9 mg in 10 mL of ethanol + 40 mL of Sorensen buffer, pH 6.96, respectively. Both solutions were stored in amber flask (to avoid photochemical degradation) and maintained in the refrigerator during one week maximum.

Cyclic voltammograms were recorded between -400 and 1200 mV, the scan rate varied from 10 to 100 mVs^{-1}. Nitrogen was used to degas the solution, and the solution was covered with a nitrogen blanket during experiments. All measurements were carried out at room temperature (25 ± 1 ^oC) and at least in triplicate, and the mean value was considered.

The oxidation procedure was performed using the stock solutions 0.25 mmol L^{-1} of HYTPHENYL, and 3.0 mmol L^{-1} of HTMCX in phosphate buffer (PBS), pH 7.14, and Sorensen buffer, pH 6.96. The oxidation peak did not disappear and cell current did not decrease. The oxidized compounds were still electroactive, with an oxidation peak at a less positive potential. In all reported experiments, the results obtained with GCE in

the presence of the HYTPHENYL and HTMCX were compared with those obtained with reference blank electrode operated under the same conditions.

2.6 Microbiological characterization

Bacterial Material

The microorganisms used in sensitivity to HYTPHENYL natural product testing were obtained from American Type Culture Collection (ATCC) by means of National Institute for Quality Control in Health (INCQS, Instituto Nacional de Controle de Qualidade em Saúde) from Oswaldo Cruz Foundation (FIOCRUZ, Fundação Oswaldo Cruz), Health Ministry, Brazil. The bacterial strains used were *Escherichia coli* 27 and *Staphylococcus aureus* 358. All strains were maintained on heart infusion agar (HIA, Difco Laboratories Ltd.). Before the tests, the strains were grown for 18 h at 35 ºC in broth brain heart infusion (BHI, Difco Laboratories Ltd.).

Antimicrobial Activity Test

The initial solution was prepared by dissolving 10 mg of the crystalline compound HYTPHENYL in 1.0 mL of dymethilsulfoxide (DMSO-Merck, Darmstadt, Germany) obtaining an initial concentration of 10 mg/mL. This initial solution was then diluted in a volume of 5.0 mL to be used in all microbiological tests. Afterwards, an aliquot of the initial solution was dissolved in DMSO to a final concentration of 1024 μg/mL.

The drugs used in the antimicrobial activity tests were the amikacin and gentamicin antibiotics (Sigma Co., St. Louis, USA). All drugs were diluted in sterile water, to concentration 5000 mg/mL. For the evaluation of the effect of the compound HYTPHENYL as modulators of resistance to the antibiotic it was used the amikacin and gentamicin aminoglycosides (Sigma Co., St. Louis, USA) as well as the bacterial strains *Escherichia coli* 27 and *Staphylococcus aureus* 358.

Minimal inhibitory concentration (MIC) was determined in a microdilution assay as described previously [32-34]. MIC was defined as the lowest concentration at which no bacterial growth was observed. For the evaluation of the HYTPHENYL compound for antibiotic resistance-modifying activity, MIC of the antibiotics was

determined in the presence or absence of the HYTPHENYL compound at sub-inhibitory concentrations CIM/8 (1.024 μg/mL).

The antibacterial effect of the compound HYTPHENYL and the modulation of antibiotic activity (both measured by the MIC) were performed using microtiter plates, using the methodology described by Coutinho et al. [35]. A growth positive control containing broth and microorganism was used in the last well of each column. Microplates were incubated for 24h at 35 ± 2 ºC. A resazurin reagent was used to indicate the presence of uninhibited bacterial growth (pink colour) or inhibition (blue colour).

3. Results and discussion

3.1. Molecular structure

Figure 2 shows the molecular structure of HYTPHENYL. This structure is compatible with our NMR data reported in the Table 1. The base structure of the HYTPHENYL molecule comprises two six-membered aromatic rings. The ring A is formed by the atoms C1′, C2′, C3′, C4′, C5′ and C6′ and the ring B is formed by the atoms C1, C2, C3, C4, C5 and C6. These two aromatic rings are joined by a three carbon α,β-unsaturated carbonyl system. Therefore, the molecular structure of HYTPHENYL is characteristic of a chalcone substance [36].

3.2. Quantum chemical parameters

The frontier molecular orbital theory developed by Kenichi Fukui in 1950's plays a key role in the understanding of the chemical reactivity [37]. The HOMO is the outermost orbital containing donor electrons. LUMO is innermost orbital containing free places to accept electrons. The chemical behavior of HYTPHENYL molecule can be predicted by the following parameters: HOMO energy, LUMO energy, energy gap ($\Delta E = E_{LUMO} - E_{HOMO}$), vertical ionization energy ($I = -E_{HOMO}$), vertical electron affinity ($A = -E_{LUMO}$), chemical potential ($\mu = -(I + A)/2$), electronegativity ($\chi = -\mu$), global hardness ($\eta = (I - A)/2$) and electrophilicity index ($\omega = \mu^2/2\eta$) [38-40]. These quantum chemical parameters for the optimized geometries of the HYTPHENYL and HTMCX compounds are given in Table 2. The graphical structures of HOMO and LUMO molecular orbitals of HYTPHENYL compound are shown in Figure 3. The values of the energy gap, hardness and chemical potential are smaller in the HYTPHENYL

compound than the values found for the HTMCX compound [25]. Therefore, the lowering in these chemical parameters indicates that the reactivity of the HYTPHENYL compound is greater than that observed in the HTMCX compound. Consequently, HYTPHENYL compound presents higher electrophilic characters than the HTMCX compound as noted in the values of electrophilicity index of these molecules (4.01 eV for HYTPHENYL against 2.68 eV for HTMCX).

The experimental UV absorption spectra of the HYTPHENYL and HTMCX compounds are shown in Fig. 4. Comparing these spectra we see that Peak 1 remains essentially unchanged, whereas Peak 2 might have its intensity decreased due the formation of the enone chain (Cβ=Cα-C=O) of the HYTPHENYL chalcone, and Peak 3 corresponds to the new moiety (ring B).

The electrostatic surface map for HYTPHENYL compound is given in Figure 5. In this image, blue and pink regions indicate positive and negative charge distributions, respectively. In the blue regions are spread over the hydrogen atoms and methyl groups comprising the electrophilic sites of the compound HYTPHENYL. Whereas, the pink regions, where the oxygen atoms are concentrated are the nucleophilic sites. Therefore, the charge distribution in the electrostatic surface map for HYTPHENYL compound shows the existence of the sites where should occur the intra and intermolecular interactions. The polar nature of this molecule can be examined by the dipole moment presented by it. The theoretical calculations showed that the value of the dipole moment for the HYTPHENYL compound is 3.90 Debye (D) while that of dipole moment of HTMCX was 4.02 D [25]. Therefore, the HTMCX compound is only slightly more polar than the HYTPHENYL compound.

3.3. Vibrational analysis

The HYTPHENYL molecule has 41 atoms, therefore there are 123 degrees of freedom, excluding the three rotational modes and the three translational movements are expected 117 vibrational modes.

The experimental and theoretical FT-Raman spectra of polycrystalline samples of HYTPHENYL is shown in Figure 6, whereas the FT-IR spectrum of HYTPHENYL is shown in Figure 7. A complete assignment of the vibrational modes of HYTPHENYL

is presented in the Table 3. The calculated wavenumber values, not scaled, are given in the first column, while the calculated and scaled wavenumbers are given in the second column. The third and fourth columns show the experimental FT-Raman and the experimental FT-IR wavenumbers, respectively, and the last column lists the assignments with the percentage contribution of the PED for each vibrational mode.

The Raman and infrared spectra for the HYTPHENYL sample present some bands which are also characteristic of HTMCX what is expected, since HTMCX compound is the precursor for the synthesis of HYTPHENYL compound whose ring A of HTMCX compound is preserved in the synthesis. In the Supplementary Material in Figure S3 is shown the comparative between the Raman and infrared bands of the HYTPHENYL and HTMCX compounds.

The FT-IR spectrum of HYTPHENYL shows intense transmittance bands in the wavenumber range of 1800-400 cm^{-1}. From the FT-Raman spectrum we observe that modes below 200 cm^{-1} are associated with external modes and others with internal modes as discussed below.

The assignment for HYTPHENYL compound shows that most of the bands observed through FT-Raman and FT-IR spectroscopy corresponds to a mixture of vibrational modes. Also, it is ascertained that there is a good correspondence between the scaled and experimental Raman and infrared bands. Torsional vibrations and out of plane deformations are observed in throughout region of scaled wavenumbers lower than 1000 cm^{-1} in the vibrational spectra of HYTPHENYL. It is also noted that in this region there is predominance of vibrations characteristic of the ring A in both HTMCX and HYTPHENYL compounds.

In the region of scaled wavenumber between 1000 and 1631 cm^{-1} of the Raman and infrared spectra of HYTPHENYL is observed the predominance of the stretching modes of carbon-carbon and carbon-oxygen atoms. However, in this region is also possible to observe a marked localization of bending modes of the methyl group. In fact, wagging vibrations and anti-symmetric bending of the of methyl group are clearly observed in this compound. A very strong infrared band which is associated with wagging vibration of the methyl groups of the molecule was observed at 1419 cm^{-1}, and three strong infrared bands observed at 1439, 1455 and 1468 cm^{-1} are associated with the anti-symmetric bending of methyl groups of HYTPHENYL.

The carbonyl (C=O) stretching vibrations of HYTPHENYL molecular structure appear associated with stretching modes of carbon-carbon group. In the HTMCX compound these modes are restricted to two vibrational modes observed in both Raman and infrared spectra which are localized at scaled wavenumbers 1595 and 1619 cm^{-1}. On the other hand, in the HYTPHENYL compound the carbonyl (C=O) stretching mode appears associated with the ketone group CαCβ and is observed in both Raman and infrared spectra at scaled wavenumber 1429 cm^{-1}. It is noteworthy that the stretching modes of the C=O carbonyl in the IR spectra have lower intensity than those observed in other classes of organic compounds.

In the wavenumber region higher than 2800 cm^{-1} of both Raman and infrared spectra of the HYTPHENYL are expected the vibrations associated with stretching modes of CH, methyl and OH groups. For example, in the infrared spectrum of HYTPHENYL the bands seen at 3113 and 2972 cm^{-1} are associated respectively with the stretching modes of CH and C′H stretching according to the assignment done on the bases of DFT calculation. In this region of the Raman spectrum the profile of bands appears with low intensity but even in this manner is possible to note the presence of several bands. A complete description of all modes appearing in the Raman and infrared spectra is given in Table 3.

3.4. Voltammetric behavior of the HYTPHENYL

The electrochemical behavior of the HYTPHENYL was studied using cyclic voltammetry at a GCE, which has been the working electrode of choice in analogous studies [41]. In the Sorensen buffer, pH 6.96 and GC electrode, the HTMCX and chalcone derived HYTPHENYL give one well-defined anodic peak (E_{ap1} = 0.67 V) in the first cycle curve. Oxidation is an irreversible process confirmed by the absence of cathodic peak on reverse sweeps. Cyclic voltammograms for the HTMCX and HYTPHENYL compounds are shown in the Figure 8.

From the second scan, another anodic peak (E_{ap2}) is registered at 0.12 V and the decreasing of the anodic peak current (at E_{ap1}). On the reverse sweep, a reduction peak appears at E_{cp} = 0.06 V only if the second cycle curve has been scanned beforehand, no other peak appears between –0.4 and +1.0 V, indicating that the final oxidation product is reduced in the cathodic peak (E_{cp}); however, it cannot be further oxidized in that range of potential.

By the first cycle curves of cyclic voltammograms, anodic peak voltage (E_{ap1}) values give well-defined peaks, while its half-peak voltage ($E_{1/2}$) was calculated as the voltage at which the current equaled half of the maximum anodic peak current. For the HYTPHENYL, the anodic peak potentials (E_{ap1}) and half-peak potentials ($E_{1/2}$) are 0.67 V, and 0.041 V, respectively, as is shown in Figure 9.

More details about the process involved in the anodic peak are obtained by studying the dependence of the experimental current function (Ψ) on the scan rate and concentration of the HYTPHENYL. The Ψ may be defined as $\Psi = I_p/(A\nu^{1/2} c)$, where A is the working electrode area, in cm^2, ν corresponds to the potential scan rate in V s^{-1}, and c represents the bulk concentration of HYTPHENYL in mol L^{-1}. This parameter is more sensitive to the electrode processes [42, 43].

Typical results for different concentrations and scan rates are $\Psi \cong 1.1$ A $(V/s)^{-1/2}$ cm^{-2} L mol^{-1}. The estimated number (with 10 % of error) of electrons exchanged in the overall electrode process can be calculated by using the experimental Ψ value and comparing with model compounds that exchange one and two electrons measured with the same working electrode in similar experimental conditions.

Potassium ferrocyanide was selected as a model for one-electron exchange Ψ = 0.68 A $(V/s)^{-1/2}$ cm^{-2} L mol^{-1}, and 1,4-hydroquinone as a two-electron exchange model [38], Ψ = 1.4 A $(V/s)^{-1/2}$ cm^{-2} L mol^{-1}. The value of $\Psi \cong 1.2$ A $(V/s)^{-1/2}$ cm^{-2} L mol^{-1} indicates that the overall electrode process for HYTPHENYL involves two electrons per molecule. These data lead to the conclusion that in the Sorensen buffer, pH 6.96, the oxidation of HYTPHENYL may comprise two successive one electron transfers at similar formal potential. Thus being $E^0_1 \cong E^0_2$, only one peak is detected in the first anodic scan [44].

A proposed oxidation mechanism for the HYTPHENYL compound involves the formation of a phenoxyl radical resulting from the one-electron abstraction from the 2′-hydroxyl group followed by abstraction of H^+ ion. Subsequently, this phenoxyl radical most probably forms a dimer. [45]. The introduction of another aromatic ring B on structure of the HTMCX seems to affect the oxidation capacity of the HYTPHENYL, because this compound is more easily oxidized (E_{ap} = 0.67 ± 0.04 V) than HTMCX compound (E_{ap} = 0.92 ± 0.02 V), Figure 8.

A plausible explanation for this observation is that the presence of electron-donating phenyl group (ring B) increases the electron density of the ring thus increasing the strength of the hydrogen bond between the hydrogen of the hydroxyl group and the oxygen of the carbonyl (C=O), hindering the removal of hydrogen. Finally, a good linearity (r = 0.990) for the relationship of the anodic peak current and square root of scan rate was achieved, which indicates diffusion control of HYTPHENYL oxidation on the GCE surface.

3.5. Antimicrobial activity and modulatory antibiotic activity

The MIC of the HYTPHENYL compound was 1024 μg/L for all bacterial strains tested, thereby no antibacterial activity was detected, revealing it as inactive against the microorganisms tested. However, modulatory activity of antibiotics was observed to HYTPHENYL compound against strains of *Escherichia coli* 27 and *Staphylococcus aureus* 358.

In the determination of MIC, an effect is regarded as synergistic when a favorable contribution is observed in the action of the antibiotic associated with the compound, with a decreasing in the MIC. On the other hand, an antagonistic effect happens in reverse, that is, occurs an increasing in the MIC on account the action of the antibiotic associated with the compound.

The MIC of the amikacin aminoglycoside in the presence of the HYTPHENYL compound in the MIC/8 concentration (128 μg/mL), against strains of *Escherichia coli* 27 and *Staphylococcus aureus* 358 showed a significant inhibitory effect with significance with $p < 0.01$ on the bacterial growth, as can be seen in Figure 10. These results indicate that the HYTPHENYL compound showed synergistic effects against these bacteria strains when it is associated with amikacin antibiotic.

It is worth mentioning that chalcone derivative have been used in preparation of drug for providing antibacterial activity against gram-positive bacteria, preferably methicillin-resistant *Staphylococcus aureus* [46]. In the MIC of the gentamicin aminoglycoside in the presence and absence of the HYTPHENYL compound in the MIC/8 concentration (128 μg/mL) is observed a synergy against strain of *Escherichia coli* 27 and no effect on the bacterial growth was detected against strain of *Staphylococcus aureus* 358, as can be seen in Figure 11.

Recent studies have shown that the natural product HTMCX (which is the precursor of synthesis of HYTPHENYL compound) presents synergism against strains of *Pseudomonas aeruginosa* 03 and *Staphylococcus aureus* 358 in the association with the amikacin aminoglycoside [21]. On the other hand, no effect on the bacterial growth was detected against strains of *Escherichia coli* 27 and *Staphylococcus aureus* 358 when the natural product HTMCX was associated with the gentamicin antibiotic [21].

Therefore, the combination of this new chalcone HYTPHENYL with the gentamicin and amikacin aminoglycosides may be useful for the treatment against strains of *Escherichia coli* 27 and *Staphylococcus aureus* 358.

4. Conclusions

In this work a novel chalcone HYTPHENYL was synthesized by the condensation reaction of Claisen-Schmidt in basic medium between the natural compound HTMCX and benzaldehyde and its molecular structure was determined by Nuclear Magnetic Resonance. Additionally, we have reported for the first time the vibrational spectra of polycrystalline samples of HYTPHENYL by FT-IR (between 400 and 3200 cm^{-1}) and FT-Raman (between 0 and 3200 cm^{-1}) spectroscopy. DFT calculations were performed, using the Gaussian 09 package with the B3LYP functional and 6-31G(d,p) basis set, in order to obtain information about the normal modes of vibrations, allowing a complete assignment, and several quantum chemical parameters of the HYTPHENYL chalcone. From the voltammetric study was possible to obtain an understanding for the electrochemical mechanism in aqueous medium of the HTMCX and HYTPHENYL. Antimicrobial and modulatory antibiotic activities of the HYTPHENYL compound were investigated. Significant modulatory activity of the antibiotics tested was observed for HYTPHENYL against strains of *Escherichia coli* 27 and *Staphylococcus aureus* 358. The HYTPHENYL showed synergistic effects against these bacteria strains when associated with amikacin antibiotic. Other synergistic effect could be observed for *Escherichia coli* 27 in the presence of HYTPHENYL with the gentamicin antibiotic. It is important to note that, in previous results, HTMCX did not show antimicrobial modulatory activity against *Escherichia coli* when associated with the gentamicin antibiotic. Therefore, these results demonstrate that HYTPHENYL

compound presents potential antimicrobial activity and may contribute to the control of *Escherichia coli* and *Staphylococcus aureus* bacterial resistance.

Acknowledgments

We thank CENAPAD-SP for the use of the *Gaussian09* software package and for computational facilities made available through the project "proj373"**.** Financial support from FUNCAP and CNPq is also acknowledged. A.M.R. Teixeira, Ph.D, also acknowledges financial support from the PQ/CNPq-2015 (Grant#: 303963/2015-8). H.S. Santos acknowledges financial support from the PQ-BPI/FUNCAP (Grant#: BP2-0107- 00026.01.00/15). D.M. Sena Jr. acknowledges financial support from PQ/CNPq-2017 (Grant#: 313407/2017-7). P.T.C. Freire thanks financial support from PRONEX FUNCAP/CNPq (Grant#: PR2-0101-00006.01.00/15). Authors also acknowledge Dr. Antonio César Honorato Barreto for the support in the spectroscopy measurements.

References

[1] L.D. Chiaradia, R. dos Santos, C.E. Vitor, A.A. Vieira, P.C. Leal, R.J. Nunes, J.B. Calixto, R.A. Yunes, Synthesis and pharmacological activity of chalcones derived from 2,4,6-trimethoxyacetophenone in RAW 264.7 cells stimulated by LPS: Quantitative structure–activity relationships, Bioorganic & Medicinal Chemistry, 16 (2008) 658-667.
[2] U. Berar, Chalcones: compounds possessing a diversity in applications, Orbital - The Electronic Journal of Chemistry; Orbital - Vol. 4 No. 3 - July-September 2012, DOI (2012).
[3] P. Singh, A. Anand, V. Kumar, Recent developments in biological activities of chalcones: A mini review, European Journal of Medicinal Chemistry, 85 (2014) 758-777.
[4] N. Abu, W.Y. Ho, S.K. Yeap, M.N. Akhtar, M.P. Abdullah, A.R. Omar, N.B. Alitheen, The flavokawains: uprising medicinal chalcones, Cancer Cell International, 13 (2013) 102.
[5] S. Ashraf, S. Hameed, M.N. Tahir, M.M. Naseer, Synthesis and crystal structure of bis-chalcone-derived fused-ring pyrazoline having an unusual substitution pattern, Monatshefte für Chemie - Chemical Monthly, 148 (2017) 1871-1875.
[6] A. Abbas, S. Kalsoom, T.B. Hadda, M.M. Naseer, Evaluation of 4-alkoxychalcones as a new class of antiglycating agents: a combined experimental and docking study, Research on Chemical Intermediates, 41 (2015) 6443-6462.
[7] B. Murtaza, A. Abbas, A. Aslam, M.S. Akhtar, S. Bashir, M. Khalid, M.M. Naseer, Evaluation of in vivo hypoglycemic potential of 4-ethyloxychalcone in alloxan-induced diabetic rats, Research on Chemical Intermediates, 42 (2016) 4161-4170.

[8] A. Abbas, H. Gökce, S. Bahceli, M. Bolte, M.M. Naseer, Solid state structural and theoretical investigations of a biologically active chalcone, J. Mol. Struct., 1112 (2016) 124-135.
[9] A. Abbas, H. Gökce, S. Bahçeli, M.M. Naseer, Spectroscopic (FT-IR, Raman, NMR and UV–vis.) and quantum chemical investigations of (E)-3-[4-(pentyloxy)phenyl]-1-phenylprop-2-en-1-one, J. Mol. Struct., 1075 (2014) 352-364.
[10] F. Anam, A. Abbas, K.M. Lo, S. Hameed, P. Ramasami, Y. Umar, A. Ullah, M.M. Naseer, Synthesis, crystal structure, experimental and theoretical investigations of 3-(4-ethoxy-3-methoxyphenyl)-1-phenylprop-2-en-1-one, J. Mol. Struct., 1127 (2017) 742-750.
[11] C.W. Mai, M. Yaeghoobi, N. Abd-Rahman, Y.B. Kang, M.R. Pichika, Chalcones with electron-withdrawing and electron-donating substituents: Anticancer activity against TRAIL resistant cancer cells, structure–activity relationship analysis and regulation of apoptotic proteins, European Journal of Medicinal Chemistry, 77 (2014) 378-387.
[12] R.J. Anto, K. Sukumaran, G. Kuttan, M.N.A. Rao, V. Subbaraju, R. Kuttan, Anticancer and antioxidant activity of synthetic chalcones and related compounds, Cancer Letters, 97 (1995) 33-37.
[13] A. Sharma, B. Chakravarti, M.P. Gupt, J.A. Siddiqui, R. Konwar, R.P. Tripathi, Synthesis and anti breast cancer activity of biphenyl based chalcones, Bioorganic & Medicinal Chemistry, 18 (2010) 4711-4720.
[14] H. Sharma, S. Patil, T.W. Sanchez, N. Neamati, R.F. Schinazi, J.K. Buolamwini, Synthesis, biological evaluation and 3D-QSAR studies of 3-keto salicylic acid chalcones and related amides as novel HIV-1 integrase inhibitors, Bioorganic & Medicinal Chemistry, 19 (2011) 2030-2045.
[15] M. Gabor, J. Sallai, T. Szell, G. Sipos, Relation of antibacterial activity and chemical structure of chalcone derivatives, Acta Microbiologica Academiae Scientiarum Hungaricae, 14 (1967) 45-&.
[16] S.A. Khan, Green Synthesis, Spectrofluorometric Characterization and Antibacterial Activity of Heterocyclic Compound from Chalcone on the Basis of in Vitro and Quantum Chemistry Calculation, Journal of Fluorescence, 27 (2017) 929-937.
[17] A. Kumar, D. Paliwal, D. Saini, A. Thakur, S. Aggarwal, D. Kaushik, A comprehensive review on synthetic approach for antimalarial agents, European Journal of Medicinal Chemistry, 85 (2014) 147-178.
[18] Z. Nowakowska, A review of anti-infective and anti-inflammatory chalcones, Eur J Med Chem, 42 (2007).
[19] L.D. Chiaradia, P.G.A. Martins, M.N.S. Cordeiro, R.V.C. Guido, G. Ecco, A.D. Andricopulo, R.A. Yunes, J. Vernal, R.J. Nunes, H. Terenzi, Synthesis, Biological Evaluation, And Molecular Modeling of Chalcone Derivatives As Potent Inhibitors of Mycobacterium tuberculosis Protein Tyrosine Phosphatases (PtpA and PtpB), Journal of Medicinal Chemistry, 55 (2012) 390-402.
[20] P. Boeck, P.C. Leal, R.A. Yunes, V. Cechinel, S. Lopez, M. Sortino, A. Escalante, R.L.E. Furlan, S. Zacchino, Antifungal activity and studies on mode of action of novel xanthoxyline-derived chalcones, Arch. Pharm., 338 (2005) 87-95.
[21] M.T.A. Oliveira, A.M.R. Teixeira, H.D.M. Coutinho, I.R.A. Menezes, D.M. Sena, Jr., H.S. Santos, B.M. de Mesquita, M.R.J.R. Albuquerque, P.N. Bandeira, R. Braz Filho, Identification and Modulatory Activity Assessment of 2-Hydroxy-3,4,6-trimethoxyacetophenone Isolated from Croton anisodontus Mull. Arg.(Euphorbiaceae), Nat. Prod. Commun., 9 (2014) 665-668.

[22] A.C.S.S. Bernardino, A.M.R. Teixeira, J.E.S.A. de Menezes, C.C.C. Pinto, H.S. Santos, P.T.C. Freire, H.D.M. Coutinho, D.M. Sena Junior, P.N. Bandeira, R. Braz-Filho, Spectroscopic and microbiological characterization of labdane diterpene 15,16-epoxy-4-hydroxy-labda-13(16),14-dien-3,12-dione isolated from the stems of Croton jacobinensis, J. Mol. Struct., 1147 (2017) 335-344.
[23] M.E. Maier, Design and synthesis of analogues of natural products, Organic & Biomolecular Chemistry, 13 (2015) 5302-5343.
[24] A.S. Ivanov, Meldrum's acid and related compounds in the synthesis of natural products and analogs, Chem. Soc. Rev., 37 (2008) 789-811.
[25] R.N.S. Santiago, P.T.C. Freire, A.P. Ayala, A.M.R. Teixeira, H.S. Santos, P.N. Bandeira, F.G. Gonçalves, M.T.A. Oliveira, B.G. Cruz, D.M. Sena Jr, Crystal structure, vibrational spectra and quantum chemical parameters of 2-hydroxy-3,4,6-trimethoxyacetophenone isolated from the Croton anisodontus Müll. Arg. (Euphorbiaceae), J. Mol. Struct., 1171 (2018) 815-826.
[26] Z. Wang, Comprehensive Organic Name Reactions and Reagents, John Wiley and Sons, Inc.2009.
[27] M.J. Frisch, G.W. Trucks, H.B. Schlegel, G.E. Scuseria, M.A. Robb, J.R. Cheeseman, G. Scalmani, V. Barone, B. Mennucci, G.A. Petersson, H. Nakatsuji, M. Caricato, X. Li, H.P. Hratchian, A.F. Izmaylov, J. Bloino, G. Zheng, J.L. Sonnenberg, M. Hada, M. Ehara, K. Toyota, R. Fukuda, J. Hasegawa, M. Ishida, T. Nakajima, Y. Honda, O. Kitao, H. Nakai, T. Vreven, J.A. Montgomery Jr., J.E. Peralta, F. Ogliaro, M.J. Bearpark, J. Heyd, E.N. Brothers, K.N. Kudin, V.N. Staroverov, R. Kobayashi, J. Normand, K. Raghavachari, A.P. Rendell, J.C. Burant, S.S. Iyengar, J. Tomasi, M. Cossi, N. Rega, N.J. Millam, M. Klene, J.E. Knox, J.B. Cross, V. Bakken, C. Adamo, J. Jaramillo, R. Gomperts, R.E. Stratmann, O. Yazyev, A.J. Austin, R. Cammi, C. Pomelli, J.W. Ochterski, R.L. Martin, K. Morokuma, V.G. Zakrzewski, G.A. Voth, P. Salvador, J.J. Dannenberg, S. Dapprich, A.D. Daniels, Ö. Farkas, J.B. Foresman, J.V. Ortiz, J. Cioslowski, D.J. Fox, Gaussian 09, Gaussian, Inc., Wallingford, CT, USA, 2009.
[28] ACD/Structure Viewer - Freeware version 2016.1.1., Advanced Chemistry Development, Inc., Toronto, ON, Canada, 2016.
[29] G.A. Andrienko, Chemcraft, www.chemcraftprog.com.
[30] G. Rauhut, P. Pulay, Transferable Scaling Factors for Density Functional Derived Vibrational Force Fields, The Journal of Physical Chemistry, 99 (1995) 3093-3100.
[31] M.H. Jamroz, J.C. Dobrowolski, Potential energy distribution (PED) analysis of DFT calculated IR spectra of the most stable Li, Na, and Cu(I) diformate molecules, J. Mol. Struct., 565 (2001) 475-480.
[32] M.M. Javadpour, M.M. Juban, W.-C.J. Lo, S.M. Bishop, J.B. Alberty, S.M. Cowell, C.L. Becker, M.L. McLaughlin, De Novo Antimicrobial Peptides with Low Mammalian Cell Toxicity, Journal of Medicinal Chemistry, 39 (1996) 3107-3113.
[33] NCCLS: Methods for Dilution Antimicrobial Susceptibility Tests for Bacteria That Grow Aerobically;Approved Standard, National Committee for Clinical Laboratory Standards, Wayne, PA, 2003, pp. 14 - 18.
[34] CLSI - Clinical and Laboratory Standards Institute, Reference Method for Broth Dilution Antifungal Susceptibility Testing of Filamentous Fungi. Approved Standard M27-A2., 5ª ed., NIH, Wayne, PA, USA, 2002.
[35] H.D.M. Coutinho, J.G.M. Costa, E.O. Lima, V.S. Falcao-Silva, r.J.P. Siqueira-Junio, In vitro interference of Momordica charantia and chlorpromazine in the resistance to aminoglycosides, Pharmaceutical Biology, 47 (2008) 1056-1059.

[36] A. Patra, G. Ghosh, P.K. Sengupta, S. Nath, C-13 NMR SPECTRAL STUDIES ON CHALCONES AND ACETOPHENONES, Magn. Reson. Chem., 25 (1987) 734-742.
[37] K. Fukui, The Role of Frontier Orbitals in Chemical Reactions (Nobel Lecture), Angewandte Chemie International Edition in English, 21 (1982) 801-809.
[38] R.G. Parr, Functional Theory of Atoms and Molecules, Oxford University Press, New York, 1989.
[39] R.G. Parr, L. Von Szentpaly, S.B. Liu, Electrophilicity index, J. Am. Chem. Soc., 121 (1999) 1922-1924.
[40] R.G. Parr, R.G. Pearson, Absolute hardness - companion parameter to absolute electronegativity, J. Am. Chem. Soc., 105 (1983) 7512-7516.
[41] S. Mannino, O. Brenna, S. Buratti, M.S. Cosio, A New Method for the Evaluation of the 'Antioxidant Power' of Wines, Electroanalysis, 10 (1998) 908-912.
[42] A.J. Bard, L.R. Faulkner, Electrochemical Methods: Fundamentals and Applications, Wiley, New York, 2001.
[43] A.A.J. Torriero, C.E. Tonn, L. Sereno, J. Raba, Electrooxidation mechanism of non-steroidal anti-inflammatory drug piroxicam at glassy carbon electrode, Journal of Electroanalytical Chemistry, 588 (2006) 218-225.
[44] D.S. Polcyn, I. Shain, Multistep Charge Transfers in Stationary Electrode Polarography, Analytical Chemistry, 38 (1966) 370-375.
[45] N. Cotelle, P. Hapiot, J. Pinson, C. Rolando, H. Vézin, Polyphenols Deriving from Chalcones: Investigations of Redox Activities, The Journal of Physical Chemistry B, 109 (2005) 23720-23729.
[46] H. Liu, Y. Wang, E. Zhang, M. Wang, P. Wang, S. Wang, D. Zhao, S. Qin, M. Zhou, P. Bai, D. Cui, Y. Hua, S. Xu, New chalcone derivative useful in preparation of drug for providing antibacterial activity against gram-positive bacteria, preferably methicillin-resistant Staphylococcus aureus, Univ Zhengzhou (UYZH-Non-standard).

CAPTION FOR THE FIGURES:

Figure 1: Scheme of the synthesis of the HYTPHENYL chalcone.

Figure 2. Molecular structure in ball and stick model with atom numbering for HYTPHENYL.

Figure 3: The frontier HOMO and LUMO orbitals for the HYTPHENYL chalcone.

Figure 4: Experimental UV absorption spectra of the HYTPHENYL and HTMCX compounds.

Figure 5: The electrostatic surface map for the HYTPHENYL chalcone.

Figure 6: Experimental and theoretical FT-Raman spectra of the HYTPHENYL in the spectral range from 3200–2600 cm^{-1} and 1800–0 cm^{-1}.

Figure 7: Experimental FT-IR spectrum of the HYTPHENYL in the spectral range from 3200–2500 cm^{-1} and 1800–400 cm^{-1}.

Figure 8: Cyclic voltammograms recorded on GCE in: (—) Sorensen buffer, pH 6.96, with (—) HYTPHENYL 25 μmol L^{-1} and (—) HTMCX 300 μmol L^{-1}. Experimental conditions: $E_{initial} = E_{final}$ = –0,40 V; $E_{\lambda 1}$ = 1,20 V; $E_{\lambda 2}$ = –0,40 V. Scan rate: (A) 10 mVs^{-1} and (B) 100 mVs^{-1}.

Figure 9: Cyclic voltammograms recorded on GCE in: (···) blank, HYTPHENYL 25 μmolL^{-1} with (—) PBS, pH 7.14, and (—) Sorensen buffer, pH 6.96. Experimental conditions: $E_{initial} = E_{final}$ = –0,40 V; $E_{\lambda 1}$ = 1,00 V; $E_{\lambda 2}$ = –0,40 V. Scan rate: (A) 10 mVs^{-1} and (B) 100 mVs^{-1}.

Figure 10: Minimum inhibitory concentration (MIC) of amikacin aminoglycoside in the presence and absence of the HYTPHENYL compound in a MIC/8 concentration

(128 μg/mL) towards *Escherichia coli 27 and Staphylococcus aureus 358*. Statistically significant value with **p<0.01.

Figure 11: Minimum inhibitory concentration (MIC) of gentamicin aminoglycoside in the presence and absence of the HYTPHENYL compound in a MIC/8 concentration (128 μg/mL) towards *Escherichia coli 27 and Staphylococcus aureus 358*. Statistically significant value with ***p<0.001.

CAPTION FOR THE TABLES:

Table 1: ^{1}H and ^{13}C NMR data for the HYTPHENYL chalcone (in $CDCl_3$), J in Hz. Chemical displacements δ_C and δ_H are in ppm.

Table 2: Quantum chemical parameters for the optimized geometries of HYTPHENYL and HTMCX compounds (eV).

Table 3: Calculated vibrational wavenumbers unscaled and scaled by the scale factors 0.9626 (20 cm^{-1} to 2000 cm^{-1}) and 0.9440 (2000 cm^{-1} to 4000 cm^{-1}), experimental Raman and transmittance band positions and assignment of vibrational modes for the HYTPHENYL.

SUPPLEMENTARY MATERIAL

Figure S1: NMR spectrum of ^{13}C (125 MHz) in ($CDCl_3$, δ, ppm, J/Hz) for HYTPHENYL.

Figure S2: NMR spectrum of ^{1}H (500 MHz) in ($CDCl_3$, δ, ppm, J/Hz) for HYTPHENYL.

Figure S3: Comparative between the Raman and infrared bands of the HYTPHENYL and HTMCX compounds.

Table 1: ^{1}H and ^{13}C NMR data for the chalcone HYTPHENYL (in CDCl3), J in Hz. Chemical displacements δ_C and δ_H are in ppm.

C	δ_C	δ_H
1’	107.1	
2’	158.8	
3’	131.2	
4’	159.6	
5’	87.4	6.01 (s)
6’	158.7	
MeO-3	60.9	3.85 (s)
MeO-4	56.3	3.96 (s)
MeO-6	56.2	3,96 (s)
C=O	193.5	
1	135.7	
2/6	128.6	7.60 (dd, J = 7.53; 1.77 Hz)
3/5	129.1	7.43 (m)
4	130.3	7.42 (m)
C_α	127.7	7.79 (d, J = 15.60 Hz)
C_β	142.8	7.88 (d, J = 15.60 Hz)

Table 2: Quantum chemical parameters for the optimized geometries of HYTPHENYL and HTMCX compounds (eV).

Compound	E_{HOMO}	E_{LUMO}	ΔE	I	A	μ	χ	η	ω
HYTPHENYL	-5.59	-2.02	3.57	5.59	2.02	-3.81	3.81	1.79	4.01
HTMCX*	-5.67	-1.23	4.44	5.67	1.23	-3.45	3.45	2.22	2.68

*Data of HTMCX were taken from Ref. [25].

Table 3: Calculated vibrational wavenumbers unscaled and scaled by the scale factors 0.9626 (20 cm^{-1} to 2000 cm^{-1}) and 0.9440 (2000 cm^{-1} to 4000 cm^{-1}), experimental Raman and transmittance band positions and assignment of vibrational modes for the HYTPHENYL.

ω_{calc}	ω_{scal}	$\omega_{FT\text{-}Raman}$	$\omega_{FT\text{-}IR}$	**Assignment of vibrational modes for the HYTPHENYL with PED* (%)**
12	12			τ (C5′C6′C1′C) (10) + τ (C6′C1′CCα) (12) + τ (C8′O4C4′C5′) (47)
18	17			τ (C5′C6′C1′C) (18) + τ (C6′C1′CCα) (26) + τ (C8′O4C4′C5′) (17)
20	19			τ (CαCβC1C2) (59) + τ (C1′CCαCβ) (31)
47	45			δ (CαCβC1) (26) + δ (C1′CCα) (19) + δ (CCαCβ) (28)
67	64	65m		τ (C4′C5′C6′C1′) (14) + τ (C7′O5C6′C5′) (33) + τ(C1′O4C4′C5′) (12)
77	74			τ (C5′C6′C1′C) (12) + τ (C1′CCαCβ) (10) + τ (CCαCβC1) (15) + γ (CβC2C6C1) (12)
102	98	86m		τ (C2′C3′C4′C5′) (20) + τ (C7′O5C6′C5′) (11) + τ (C9′O3C3′C4′) (15)
103	99			τ (C7′O5C6′C5′) (12) + τ (C9′O3C3′C4′) (32)
111	107			τ (C3′C4′C5′C6′) (10) + τ (C1′CCαCβ) (23) + τ (C9′O3C3′C4′) (12)
121	116			τ (C6′C1′CCα) (22) + τ (C7′O5C6′C5′) (14)
147	142	137vw		δ (O3C3′C2′) (12) + τ (HC9′O3C3′) (27) + τ (C9′O3C3′C4′) (18)
198	191			τ (C3′C4′C5′C6′) (15) + τ (C2′C3′C4′C5′) (15) + τ (C4′C5′C6′C1′) (19) + γ (O4C5′C3′C4′) (12)
201	193			δ (C6′C1′C) (16) + δ (CβC1C6) (11) + δ (O5C6′C5′) (17) + δ (C7′O5C6′) (14)
206	198			δ (O4C4′C3′) (15) + δ (O5C6′C5′) (16)
230	221			δ (C9′O3C3′) (18) + γ (O3C4′C2′C3′) (22)
243	234			τ (HC8′O4C4′) (24) + τ (HC8′O4C4′) (19) + τ (HC8′O4C4′) (15) + τ (C2′C3′C4′C5′) (13)
264	254			δ (O4C4′C3′) (14) + δ (CβC1C6) (13) + δ (C8′O4C4′) (16)
277	267			τ (C6C5C4C3) (14) + τ (C3′C4′C5′C6′) (30) + τ (CCαCβC1) (21)
286	275	287vw		τ (HC7′O5C6′) (25) + τ(HC7′O5C6′) (14) + τ (HC7′O5C6′) (12)
312	300			τ (C5′C6′C1′C) (23) + τ (C3′C4′C5′C6′) (22)
324	312	325vw		δ (O3C3′C2′) (24)
356	343			δ (C6′C1′C) (14) + δ (C8′O4C4′) (31)
376	362			δ (C2′C3′C4′) (10) + δ (C3′C4′C5′) (16) + δ (O3C3′C2′) (11)
413	398	382vw		τ (HC2C3C4) (10) + τ (HC6C5C4) (12) + τ (C6C5C4C3) (33) + τ (C5C4C3C2) (20) + τ (C1C2C3C4) (18)
429	413	420vw	417m	ν (C1′C) (12) + δ (C4′C5′C6′) (16) +δ (C8′O4C4′) (11)
439	423			δ (O2C2′C1′) (33)
467	450	453vw	454m	δ (C7′O5C6′) (11)
498	479			γ (CβC2C6C1) (33)
501	482	487vw	486m	δ (CαCβC1) (10) + δ (C1′CCα) (15)
514	495	499vw	496vw	δ (C9′O3C3′) (23)
574	553	517vw		ν (C3′C4′) (18) + ν (O4C4′) (10) + δ (C2′C3′C4′) (15)
592	570	577vw	575s	δ (O1CCα) (26) + δ (C1C2C3) (18)
622	599	593vw	595vw	τ (HC5′C6′C1′) (23) + γ (O1C3′C1′C2′) (22) + γ (O2C5′C3′C4′) (28)
633	609			δ (C6C5C4) (22) + δ (C4C3C2) (38) + δ (C1C2C3) (13)
641	617	618vw	617m	ν (C1′C) (11) + δ (O1CCα) (10) + δ (C3′C4′C5′) (11)
655	631	630vw		γ (O1CαC1′C) (15) + γ (O5C5′C1′C6′) (40)
693	667	656vw		τ (C1C2C3C4) (13) + γ (O2C3′C1′C2′) (13) + γ (O3C4′C2′C3′) (13) + γ (O4C5′C3′C4′) (15)
701	675		688vs	τ (HC4C5C6) (10) + τ (C3′C4′C5′C6′) (10) + τ (C1C2C3C4) (26) + γ (O2C3′C1′C2′) (13)
731	704			γ (O1CαC1′C) (32)
753	725	721vw	720vs	δ (O4C4′C3′) (11) + δ (O5C6′C5′) (21)
767	738	729vw		ν (O3C3′) (14) + δ (O1CCα) (16) + δ (C5C4C3) (10)
782	753	756vw	757vs	τ (HC3C4C5) (11) + τ (HC4C5C6) (10) + τ (HC5C4C3) (11) + τ (C1C2C3C4) (17) + γ (O1CαC1′C) (13) + γ (CβC2C6C1) (13)
802	772	768vw	765vs	τ (HC5′C6′C1′) (69)
851	819	781vw		ν (CβC1) (10) + δ (C5C4C3) (19)
853	821	798vw	792vs	τ (HC2C3C4) (24) + τ (HC6C5C4) (27) + τ (HC3C4C5) (21) + τ (HC5C4C3) (19)
899	865	835vw	837s	τ (HCαCβC1) (57)
916	882	872vw	871vs	δ (CαCβC1) (11) + δ (O23CCα) (10) + δ (CCαCβ) (14)
932	897	902vw	893vs	τ (HCαCβC1) (11) + τ (HC2C3C4) (24) + τ (HC6C5C4) (22) + τ (HC4C5C6) (29)
966	930			τ (HO2C2′C3′) (92)
973	937			τ (HC2C3C4) (18) + τ (HC6C5C4) (15) + τ (HC3C4C5) (25) + τ (HC5C4C3) (33)

989	952			ν (O4C4′) (31) + ν (O3C9′) (13)
999	962	969vw	964vs	τ (HC3C4C5) (23) + τ (HC4C5C6) (30) + τ (HC5C4C3) (17) + τ (C6C5C4C3) (10)
1015	977			δ (C6C5C4) (33) + δ (C4C3C2) (16) + δ (C5C4C3) (20)
1026	988	990w	990vs	ν (O5C7′) (32) + ν (O4C8′) (13) + δ (C4′C5′C6′) (12)
1037	998	1000m	998vs	τ (HCαCβC1) (15) + τ (HCβC1C2) (70)
1045	1006		1009vs	ν (O3C9′) (50)
1056	1017	1027vw	1025m	ν (C4C3) (21) + ν (C5C4) (27)
1111	1069		1074vs	ν (C6C5) (12) + ν (C3C2) (19) + δ (HC2C3) (10) + δ (HC6C5) (12) + δ (HC4C3) (15)
1115	1073	1085s		ν (CCα) (19) + ν (O4C8′) (19)
1157	1114	1117vw	1123vs	ν (O2C2′) (16) + ν (O5C7′) (21)
1171	1127			r ($C8'H_3$) (26) + τ (HC8′O4C4′) (70)
1176	1132			r ($C7'H_3$) (26) + τ (HC7′O5C6′) (70)
1177	1133			r ($C9'H_3$) (26) + τ (HC9′O3C3′) (70)
1189	1145			δ (HC3C2) (17) + δ (HC4C3) (30) + δ (HC5C4) (16)
1209	1164	1154vw	1152vs	δ (HC2C3) (26) + δ (HC6C5) (19) + δ (HC3C2) (13) + δ (HC5C4) (15)
1218	1172			r ($C9'H_3$) (10) + τ (HC9′O3C3′) (44)
1223	1177	1181m		τ (HC8′O4C4′) (27)
1239	1193			ν (C1′C) (11) + δ (HC5′C6′) (18) + δ (HCαCβ) (13)
1240	1194			ν (C1C2) (13) + ν (CβC1) (21) + δ (HCβCα) (16)
1248	1201	1204m	1206vs	ν (O4C4′) (13) + ν (O5C6′) (14) + δ (HC5′C6′) (14)
1274	1226	1242m	1246vs	ν (C4′C5′) (13) + ν (O3C3′) (24)
1320	1271	1268s	1268vs	ν (C2′C3′) (17)
1332	1282			δ (HCβCα) (17)
1356	1305	1302vw	1287vs	ν (O2C2′) (18)
1357	1306			ν (CαCβ) (13) + ν (C1C2) (11) + δ (HCβCα) (30)
1368	1317	1318m	1317vs	δ (HC2C3) (24) + δ (HC6C5) (22) + δ (HC4C3) (13)
1381	1329		1333vs	ν (C5′C6′) (10) + δ (HCαCβ) (24)
1477	1422		1419vs	wag ($C9'H_3$) (54) + wag ($C8'H_3$) (14)
1482	1427			wag ($C9'H_3$) (10) + wag ($C8'H_3$) (11) + wag ($C7'H_3$) (34)
1490	1434			δ (HC4C3) (12) + δ_{as} ($C9'H_3$) (12)
1492	1436			δ (HC4C3) (10) + δ_{as} ($C9'H_3$) (22)
1500	1444	1440w	1439vs	δ_{as} ($C8'H_3$) (63) + τ (HC8′O4C4′) (12)
1503	1447			δ_{as} ($C9'H_3$) (19) + δ_{as} ($C8'H_3$) (15) + δ_{as} ($C7'H_3$) (24)
1504	1448			δ_{as} ($C7'H_3$) (69) + τ (HC7′O5C6′) (14)
1508	1452			δ_{as} ($C8'H_3$) (62) + τ (HC8′O4C4′) (11)
1516	1459		1455vs	δ_{as} ($C8'H_3$) (17) + δ_{as} ($C7'H_3$) (33)
1518	1461	1460vw		δ (HO2C2′) (17) + δ_{as} ($C7'H_3$) (10)
1527	1470		1468vs	δ_{as} ($C9'H_3$) (77) + τ (HC9′O3C3′) (14)
1531	1474			ν (O1C) (12) + δ_{as} ($C7'H_2$) (28) + wag ($C8'H_3$) (10)
1540	1482	1487s		δ (HC2C3) (17) + δ (HC6C5) (15) + δ (HC3C2) (15) + δ (HC5C4) (19)
1615	1555	1554vs	1558vs	ν (O1C) (20) + ν (C4′C5′) (14)
1629	1568			ν (C3C4) (15)
1632	1571	1576m	1584s	ν (C5′C6′) (12) + ν (C3′C4′) (10) + ν (C3C4) (10)
1657	1595	1596vs		ν (C6C5′) (30) + ν (C3C2) (10)
1677	1614			ν (C2′C3′) (15) + δ (HO2C2′) (30)
1694	1631	1624vs	1629vs	ν (CαCβ) (44) + ν (CO1) (13)
2871	2710			ν (O2H) (95)
3019	2850	2842vw		ν_s ($C9'H_3$) (99)
3028	2858			ν_s ($C7'H_3$) (100)
3058	2887	2882vw	2881m	ν_s ($C8'H_3$) (99)
3095	2922		2915m	ν_{as} ($C7'H_3$) (100)
3111	2937	2946vw	2946m	ν_{as} ($C9'H_3$) (100)
3137	2961			ν_{as} ($C8'H_3$) (99)
3148	2972	2975vw	2972m	ν_{as} ($C9'H_3$) (99)
3152	2975			ν_{as} ($C7'H_3$) (89)
3157	2980	2988vw	2986m	ν_{as} ($C8'H$) (98)
3177	2999	3007vw	3004m	ν (CβH) (56) + ν (C2H) (23) + ν (C3H) (10)
3180	3002			ν (CβH) (37) + ν (C3H) (15) + ν (C4H) (18) + ν (C5H) (19)
3185	3007			ν (C2H) (36) + ν (C6H) (10) + ν (C5H) (35)
3194	3015			ν (C2H) (22) + ν (C6H) (16) + ν (C3H) (19) + ν (C4H) (31) + ν (C5H) (11)

3203	3024		3021m	ν (C6H) (47) + ν (C3H) (29)
3210	3030			ν (C6H) (21) + ν (C3H) (20) + ν (C4H) (31) + ν (C5H) (23)
3255	3073	3058vw		ν (C5′H) (99)
3281	3097		3113m	ν (CαH) (99)

* Only PED values greater that 10 % are gives.

Nomenclature: τ = torsion; sc= scissoring; δ = deformation; δ_{as} = anti-symmetric bending, γ = deformation out of plane; δ_{out} = deformation out of plane; ν = stretching; ν_{as} = asymmetric stretching; ν_s = symmetric stretching. vs=very strong ; s = strong; m = medium; w = weak; vw =very weak.

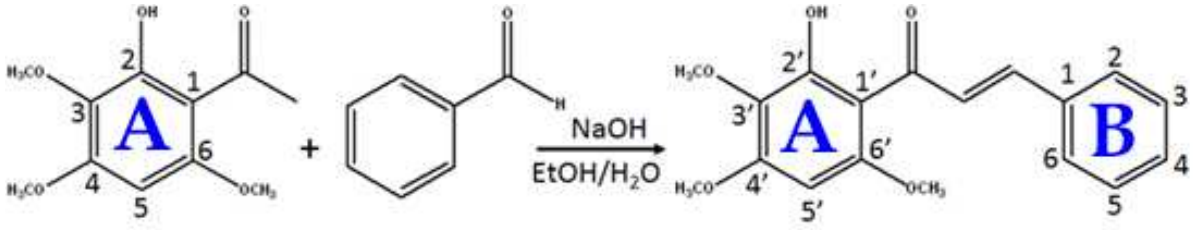

(1) (2) (3)

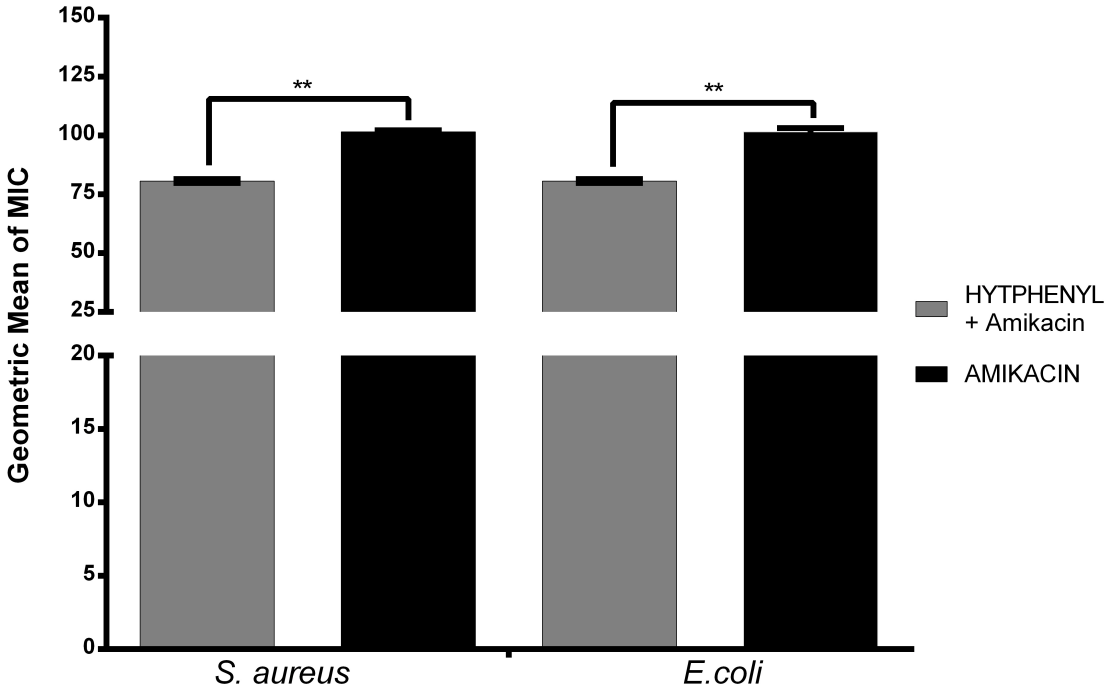

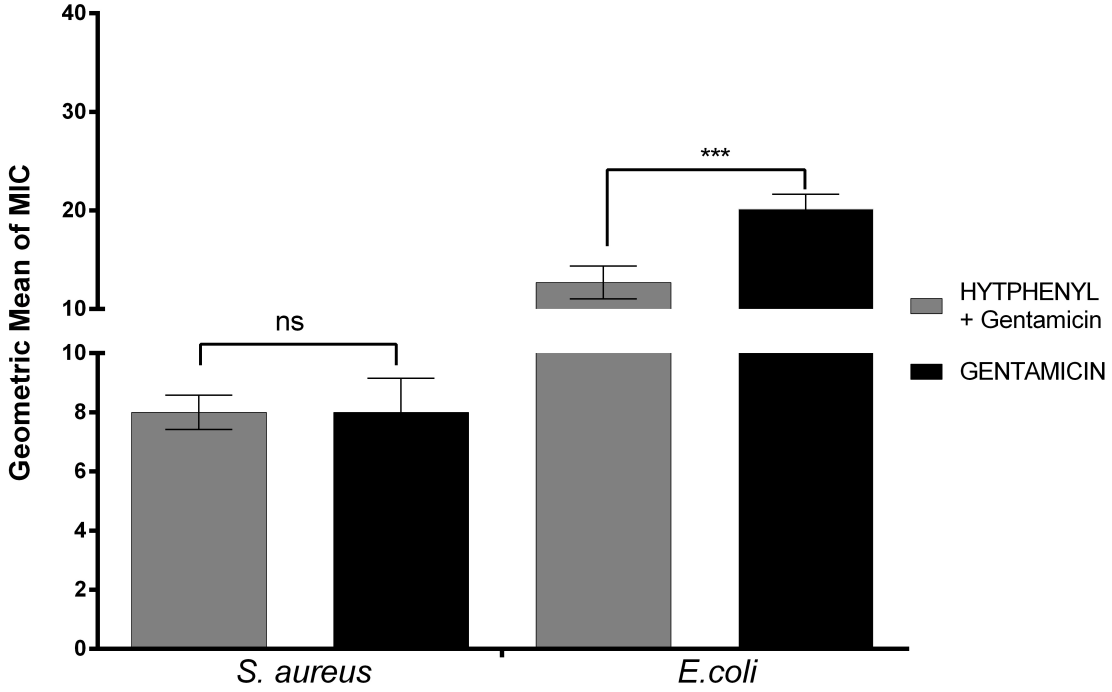

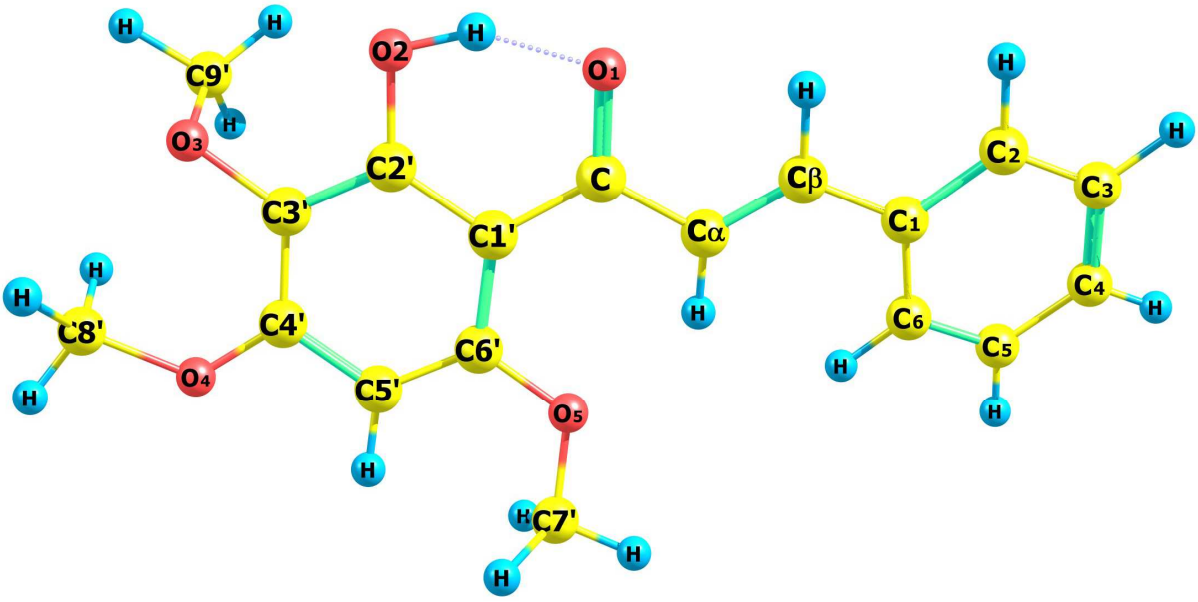

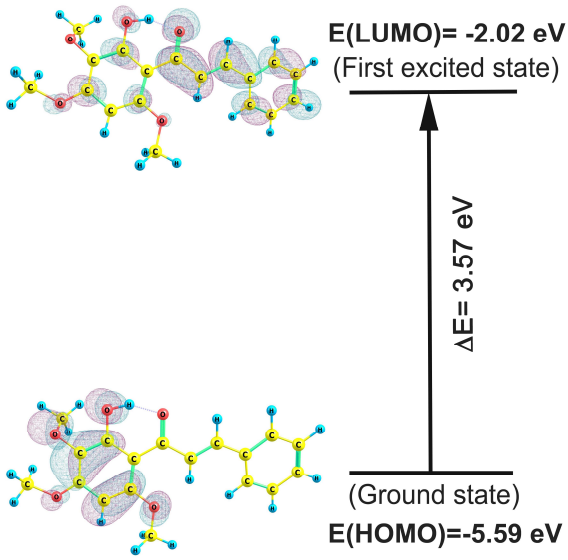

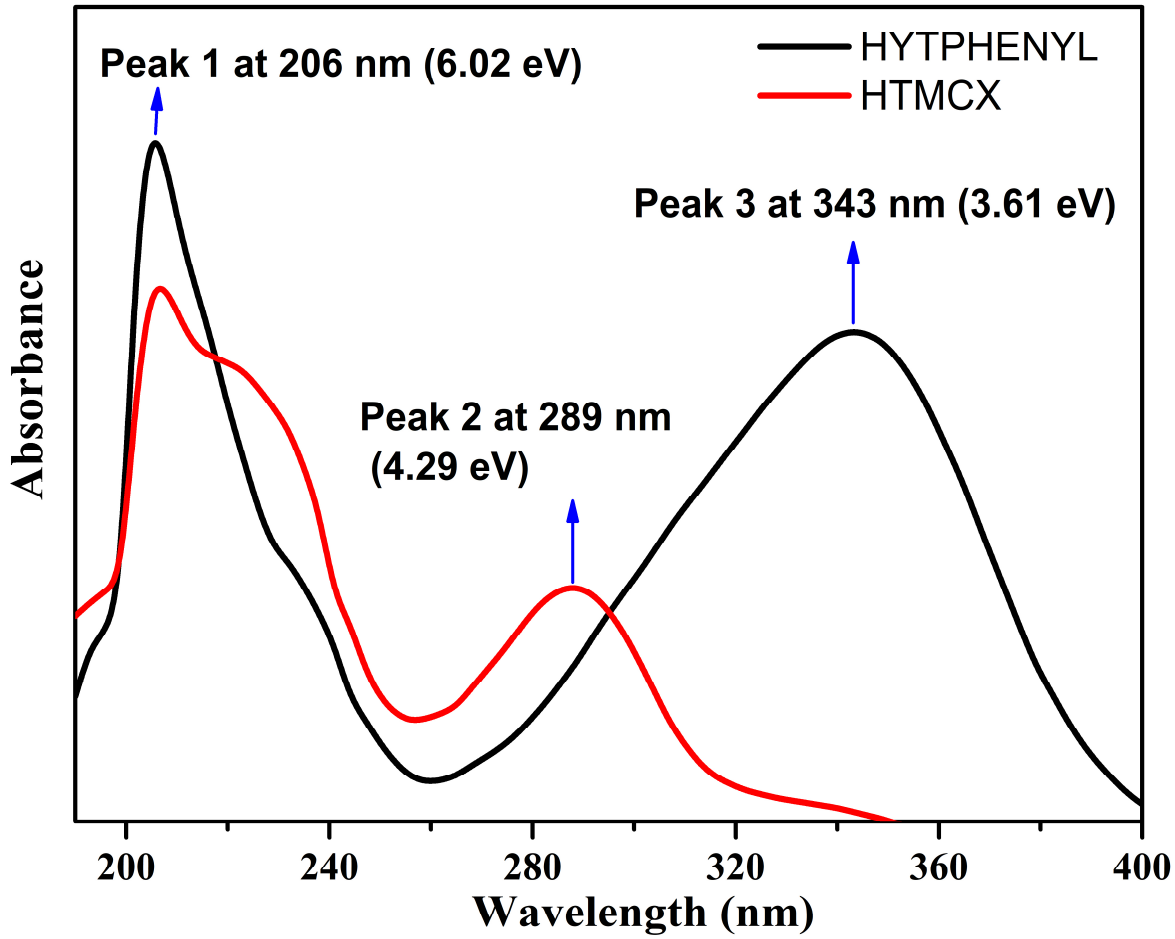
Peak 1 at 206 nm (6.02 eV)
HYTPHENYL
HTMCX
Peak 3 at 343 nm (3.61 eV)
Peak 2 at 289 nm
(4.29 eV)
Absorbance
200
240
280
320
360
400
Wavelength (nm)

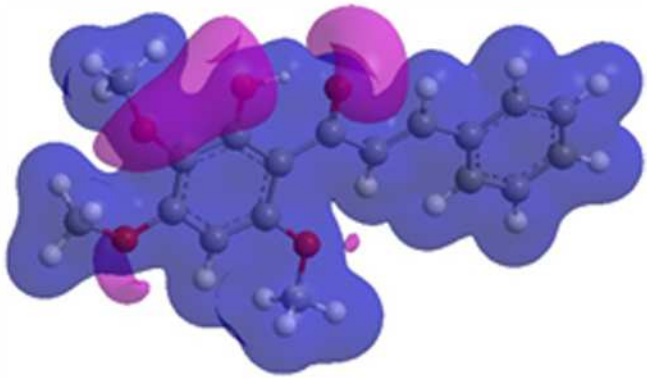

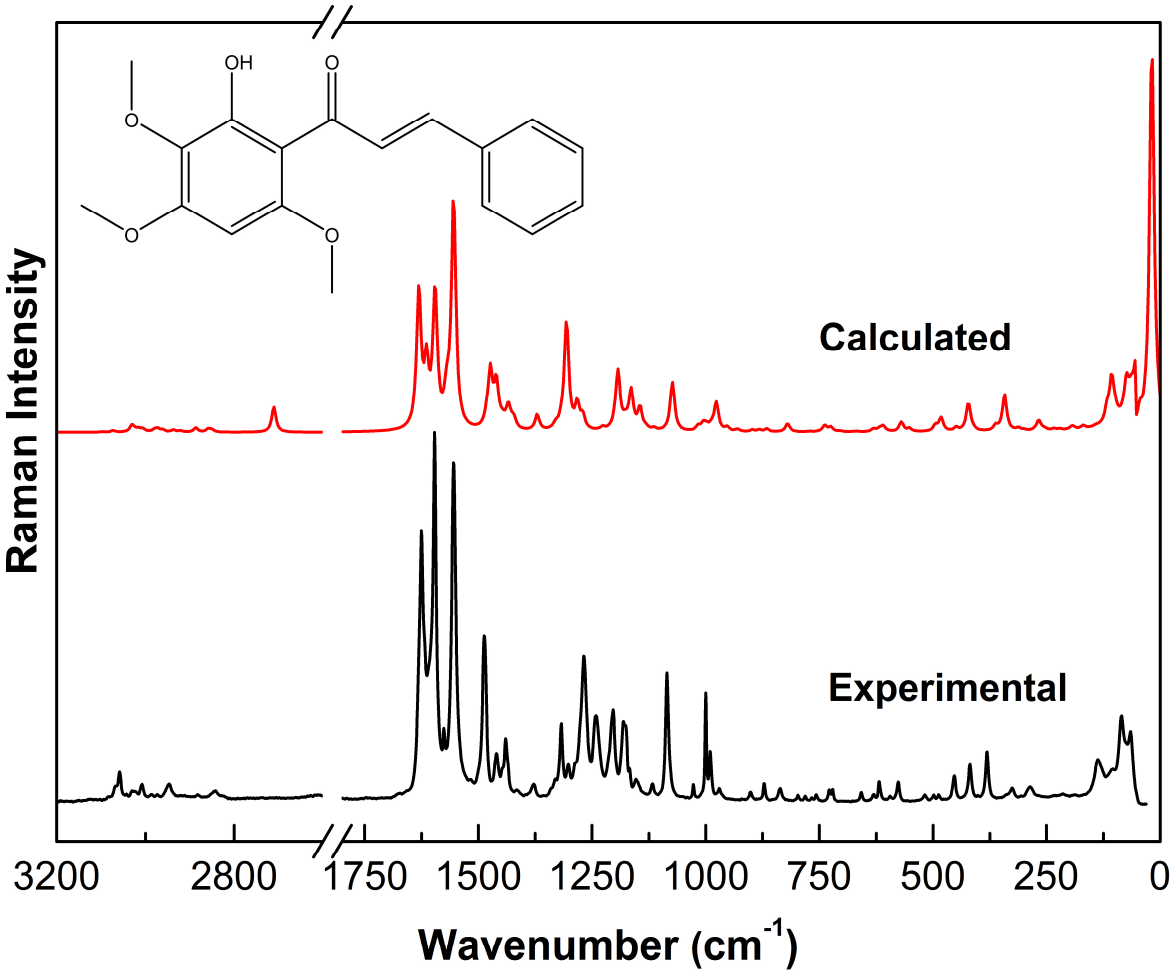
OH
O
O
O
O
Calculated
Experimental
Raman Intensity
3200
2800
1750
1500
1250
1000
750
500
250
0
Wavenumber (cm-1)

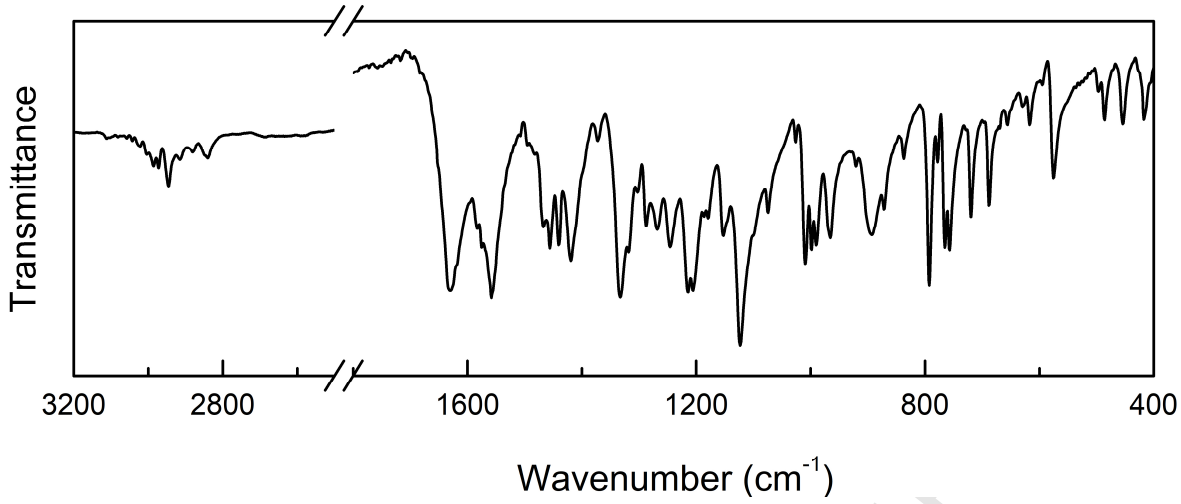

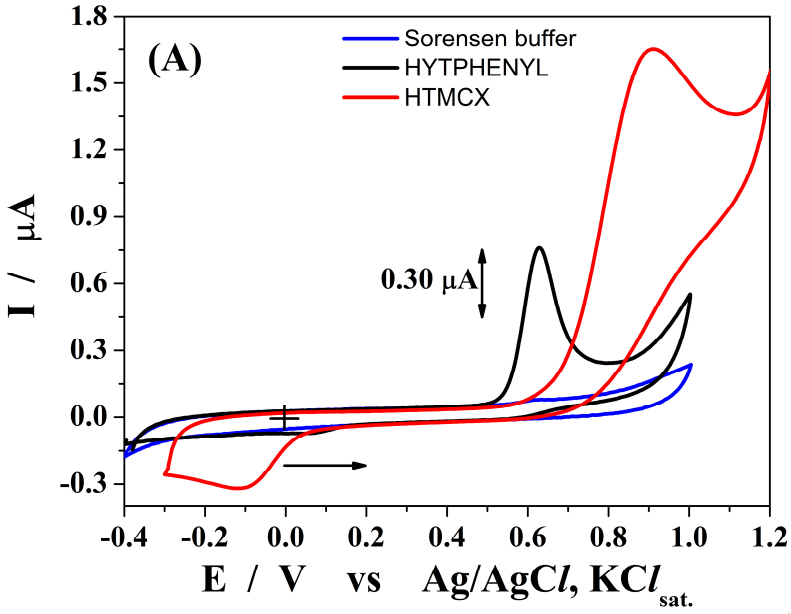
(A)
Sorensen buffer
HYTPHENYL
HTMCX
0.30 µA
I / µA
E / V vs Ag/AgCl, KCl sat.

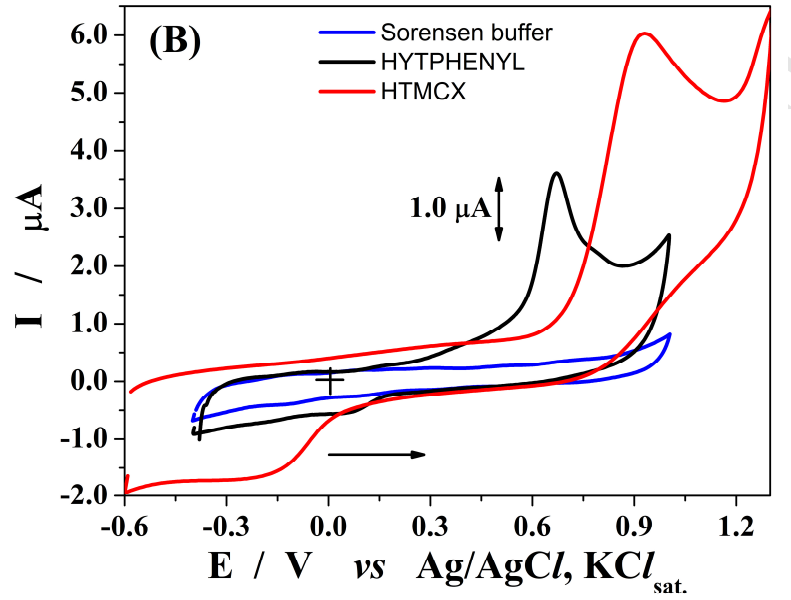
(B)
Sorensen buffer
HYTPHENYL
HTMCX
1.0 µA
I / µA
E / V vs Ag/AgCl, KCl sat.

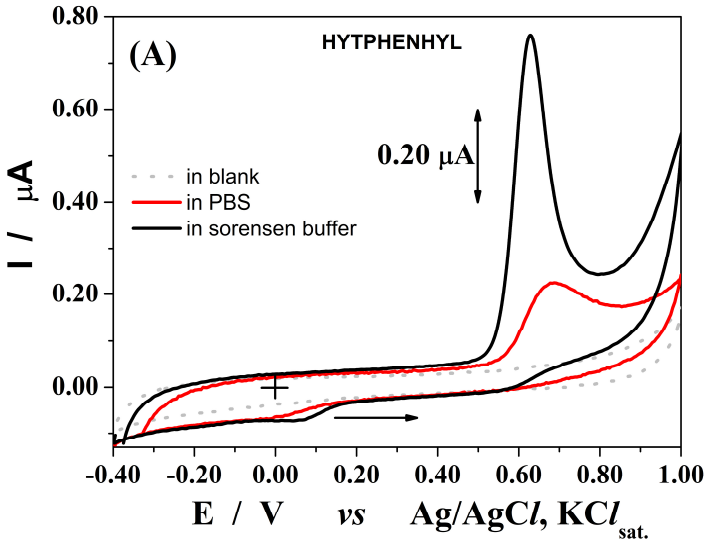

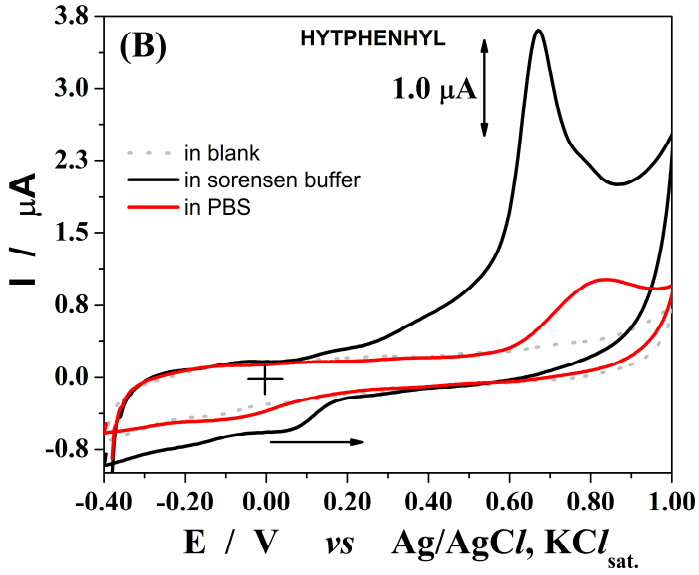

Research Highlights

- Spectroscopic characterization of a new chalcone.
- Structure was determined by NMR.
- Electrochemical study was carried out.
- Density Functional Theory, Raman and infrared studies.
- Antibacterial and modulation of antibiotic activity assays.